

No indication of chiral flux current in the topological kagome metal CsV_3Sb_5

Huazhou Li^{1,*}, Siyuan Wan^{1,*}, Han Li¹, Qing Li¹, Qiangqiang Gu¹, Huan Yang^{1,†}, Yongkai Li^{2,3}, Zhiwei Wang^{2,3}, Yugui Yao^{2,3}, and Hai-Hu Wen^{1,‡}

¹ *National Laboratory of Solid State Microstructures and Department of Physics, Collaborative Innovation Center of Advanced Microstructures, Nanjing University, Nanjing 210093, China*

² *Key Laboratory of Advanced Optoelectronic Quantum Architecture and Measurement (MOE), School of Physics, Beijing Institute of Technology, Beijing 100081, China and*

³ *Beijing Key Lab of Nanophotonics and Ultrafine Optoelectronic Systems, Beijing Institute of Technology, Beijing 100081, China*

Compounds with kagome lattice usually host many exotic quantum states, including the quantum spin liquid, non-trivial topological Dirac bands and a strongly renormalized flat band, etc. Recently an interesting vanadium based kagome family AV_3Sb_5 ($A = \text{K}, \text{Rb}, \text{or Cs}$) was discovered, and these materials exhibit multiple interesting properties, including unconventional saddle-point driven charge density wave (CDW) state, superconductivity, etc. Furthermore, some experiments show anomalous Hall effect which inspires that there might be some chiral flux current states. Here we report scanning tunneling measurements by using spin polarized tips. Although we have observed clearly the 2×2 and 1×4 CDW orders, the well-designed experiments with refined spin polarized tips do not reveal any trace of the chiral flux current phase in CsV_3Sb_5 . Thus it remains debatable whether this state really exists in CsV_3Sb_5 and we may need additional scenario to explain the anomalous Hall effect.

I. INTRODUCTION

The kagome lattice is a planar network composed of hexagons with corner-sharing triangles. Owing to its unique geometry, the antiferromagnetic (AF) long range order cannot exist due to the spin frustration, resulting in a possible quantum spin liquid state [1–4]. Large anomalous Hall effect, which is induced by the spontaneous magnetization, has been observed in some exotic AF states [5, 6] or ferromagnetic semimetals [7, 8] with the kagome lattice. In addition, materials with a kagome lattice structure can host other quantum states, such as charge density wave (CDW) [9, 10], superconductivity [10–12], topological electronic states [9, 13–18], as well as spin density wave (SDW) [19]. Recently, a new family of vanadium based metals AV_3Sb_5 ($A = \text{K}, \text{Rb}, \text{Cs}$) has been discovered with the kagome lattice consisting of vanadium atoms [20]. Subsequently, superconductivity, CDW, and topological non-trivial states are observed in these materials [21–23]. Since then, plenty of studies have been carried out on superconducting properties [24–36], the topologically non-trivial state [29, 37–39] and the CDW orders [29, 30, 38–53]. In addition, a giant anomalous Hall effect (AHE) has been observed in KV_3Sb_5 and CsV_3Sb_5 [54, 55], and this effect is detectable below the CDW transition temperature [55]. Usually, AHE breaks the time-reversal symmetry, thus a theoretical model with the hypothesis of a chiral flux current phase is proposed to explain the time-reversal symmetry breaking along c -axis direction in this family of kagome materials [56]. However, the muon spin resonance (μSR) measurement shows the absence of local magnetic moments and long-range magnetic orders in KV_3Sb_5 [57]. Besides, the electronic state does break the sixfold symmetry of the crystal structure in the ab plane. A twofold symmetry of c -axis resistivity is observed in CsV_3Sb_5 with in-plane

rotating magnetic field in both the normal and the superconducting states [58], which suggests the existence of a nematic electronic state and a twofold symmetry of superconducting gap. The nematic electronic state disappears near the CDW transition temperature [58], and it may be related to the anisotropic $2a_0 \times 2a_0$ (2×2) CDW order [30, 38, 40, 49, 51] or the $4a_0$ (1×4) unidirectional CDW order [30]. The intrinsic chiral anisotropy with the magnetic-field tunability was reported for the 2×2 CDW order in AV_3Sb_5 [40, 51], which was explained as the unconventional chiral CDW in the frustrated kagome lattice. However, the CDW order is argued to be insensitive to the magnetic field from another report [49], which seems contradicting with previous reports [40, 51]. Consequently, the conclusion about both the chiral flux current phase and tunable chiral charge order remains controversial, and they should be examined by more refined experiments, such as using the spin polarized scanning tunneling microscopy/spectroscopy (SP-STM/STS). Here, we report the measurements by using SP-STM/STS on single crystals of CsV_3Sb_5 . Within our experimental resolution, we have not found any indication of the spin texture corresponding to the proposed chiral flux current phase. Furthermore, we have neither observed any detectable spin textures of the 2×2 CDW order, which may rule out the existence of a SDW order.

II. METHODS

Single crystals of CsV_3Sb_5 were synthesized via the self-flux method [20]. The physical properties including those in superconducting and normal states were reported in a previous work [58]. The STM/STS measurements were carried out in a scanning tunneling microscope (USM-1300, Unisoku Co., Ltd.) with an ultrahigh

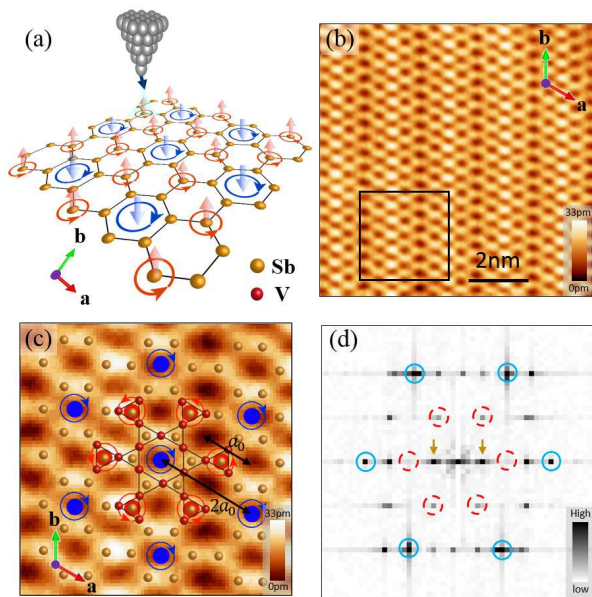


FIG. 1. (a) Schematic illustration of the spin-polarized STM measurements. (b) Atomically resolved topography of the top Sb surface ($V_{\text{set}} = 20$ mV, $I_{\text{set}} = 100$ pA). (c) Enlarged view of the topography in the area of black square in (b). The theoretically proposed hexagonal current loops are shown by blue disks, while the triangular current loops are marked by red disks. (d) Fourier transform of the topography in (b). The Bragg peaks are marked by circles; spots for the 2×2 CDW order are marked by dashed circles.

vacuum up to 1×10^{-10} torr. A typical lock-in technique is used for the spectrum and quasiparticle interference (QPI) mapping measurements with an ac modulation of 0.5 mV and a frequency of 987.5 Hz. All experimental data were taken at 4.2 K. Here we used a bulk Cr rod to make the tip for STM measurements [59]. The spin-polarized Cr tip was electrochemically etched by 3 mol/L NaOH solution with the immersed end covered by a polytetrafluoroethylene tube with a certain length [60]. After the etching, the Cr tip was transferred into the STM chamber, and then the spin polarization feature was characterized on an Fe_{1+y}Te crystal [61].

III. RESULTS

A. Modelling the topographic image with the chiral flux current phase

According to the theoretical proposal of the chiral flux current phase [56], there are two kinds of current flux loops with opposite circulating directions, and they can produce local magnetic moments with opposite vorticities in the V-Sb layer of AV_3Sb_5 . These flux loops break the time-reversal symmetry in the c -axis direction and can have different influences on the tunneling current through the spin-polarized tip with a fixed spin direc-

tion. A schematic illustration is given in Fig. 1(a). Due to the weak van der Waals interaction bridged by Cs and Sb layers, in most cases the easily exposed top layer after the cleavage is composed by Cs or Sb atoms. One can hardly obtain the V-Sb layer as the top layer. In previous STM/STS measurements, the top surface can be Sb, Cs or half Cs surfaces [29, 30, 41, 52]. Here in our measurements, the commonly obtained surface is the Sb layer, and Fig. 1(b) shows a typical atomically resolved topography of this kind of surface. The slightly elongated bright spot on the surface represents one pair of Sb atoms. Figure 1(c) shows an enlarged view of the area marked by a square in Fig. 1(b). We show together the Sb atoms on the top layer by the yellow spheres as well as those of V atoms underneath by red spheres. It is clear that the Sb atoms in the top layer form a honeycomb like structure. There are dark areas in the center of the hexagons constructed by Sb atoms. The distance between two neighbored hexagonal dark areas equals to the lattice constant a_0 in the crystal structure. If two kinds of flux loops with opposite magnetic moments existed in the V-Sb layer beneath the top Sb layer, they would locate in one quarter of the total numbers of the hexagonal and triangular vanadium plaquettes. In Fig. 1(c), the blue (red) disks denote the positions of hexagonal (triangular) current flux loops based on the theoretical proposal [56]. Here it should be noted that the hexagonal current flux loops appear only in one of every two neighboring lines of dark areas, and on this particular line they only occupy half sites. In this case, the distance between two neighboring hexagonal current flux loops is $2a_0$. Figure 1(d) shows the Fourier transformed (FT) pattern of the topography [Fig. 1(b)], and one can see several sets of spots corresponding to different periodic structures in the real space besides the Bragg peaks. In the topographic image shown in Fig. 1(b), one can see clear stripes with the period of $4a_0$. The 1×4 unidirectional order can be clearly observed as spots indicated by arrows in Fig. 1(d), and they only appear on the horizontal axis in the FT pattern. This result is similar to those from previous reports [30, 41]. The spots corresponding to the 2×2 CDW order are marked by red dashed circles in FT pattern. The intensities of these spots show a clear anisotropy, and the two spots on the horizontal axis have a relatively weaker intensity comparing to other spots.

B. Topography and tunneling spectrum with spin-polarized tips

In STM measurements, the obtained topography is a combination of the atomic height and the contribution from the density of states (DOS) [62]. As mentioned above, if the current flux loop can induce a local magnetic moment, they would affect the tunneling current through the spin-polarized tip, which is similar to the situation of investigating magnetic orders in other materials [61, 63, 64]. For effectively detecting the possible

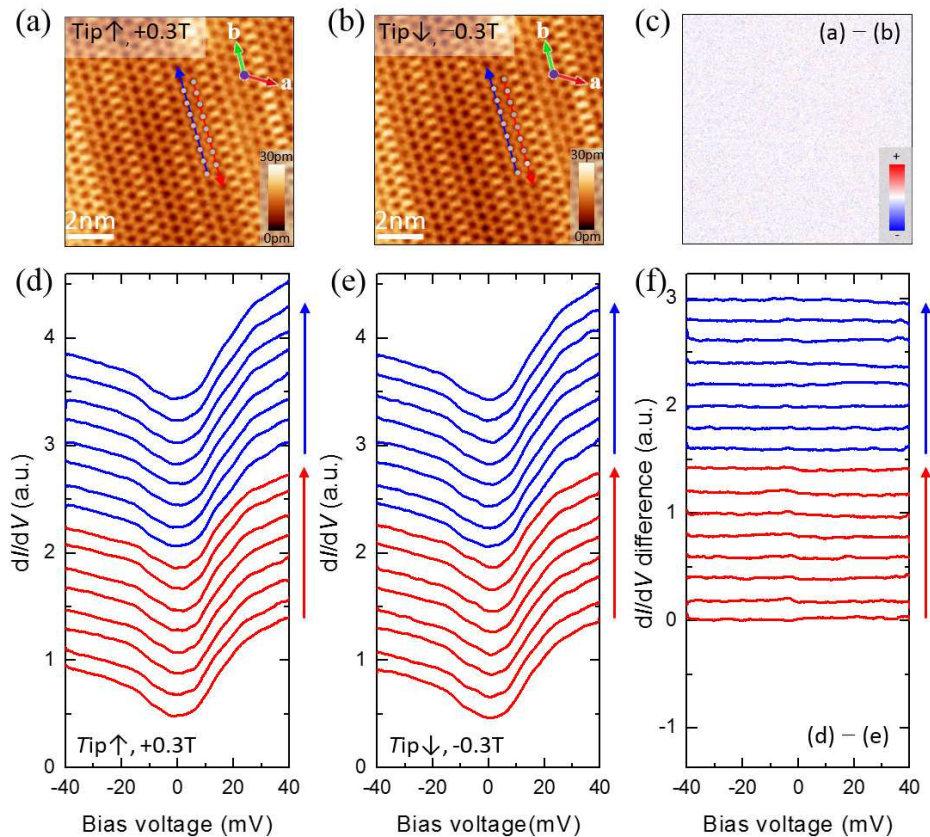


FIG. 2. (a),(b) Topography of the top Sb surface measured in the same area and under the field of +0.3 and -0.3 T; the tip has been polarized by the magnetic fields of +2 (\uparrow) and -2 T (\downarrow), respectively ($V_{\text{set}} = 30$ mV, $I_{\text{set}} = 100$ pA). (c) Spin-difference topography between the topographies shown in (a) and (b). (d),(e) Tunneling spectra taken at the centers of hexagonal holes marked by dots in (a) and (b), respectively ($V_{\text{set}} = 30$ mV, $I_{\text{set}} = 100$ pA). (f) Spin-difference spectra between the tunneling spectra taken at the same positions but with different tip spin directions and under different magnetic fields. The curves in (d) to (f) are off-set for clarity.

chiral flux current phase with a spin polarized tip, during the measurements we usually apply a small magnetic field (± 0.3 T) when the tip polarization is guaranteed. This measure is taken because we need to have a definite time-reversal symmetry breaking state if it really exists. Being different from the exotic AF state [5, 6] or ferromagnetic semimetals [7, 8] with kagome lattice, the hysteresis behavior is absent in the AHE signals measured in KV_3Sb_5 or CsV_3Sb_5 [54, 55] although a huge AHE signal is observed as a nonlinear part of the Hall resistivity. Since the Hall resistivity is zero at zero magnetic field, the spontaneous magnetization should be negligible, and the c -axis symmetry seems to be not broken in these materials at 0 T [65]. In this point of view, an external magnetic field should be applied to induce the c -axis symmetry breaking in CsV_3Sb_5 . Here in this work, the Cr tip is polarized by magnetic fields of ± 2 T. After magnetizing the tips with magnetic fields of ± 2 T, the external field is decreased to ± 0.3 T for the measurements, respectively. And the polarization direction of the tip is not changed after each magnetizing since 0.3 T is

below the reverting field (~ 0.7 T) [61]. Figures 2(a) and 2(b) show the topographic images measured at +0.3 and -0.3 T by using a Cr tip polarized by magnetic fields of +2 and -2 T, respectively. The symbol of \uparrow or \downarrow is used to denote the polarized direction of the tip. Then the spin of the tip should be opposite in these two configurations. Figure 2(c) shows the difference of the two topographic images measured with opposite spin polarizing directions. However, one cannot see any obvious periodic difference signal in the figure, which suggests that the electronic state in this area does not have detectable spin-sensitive contribution. Tunneling spectra are measured at positions in the centers of hexagonal dark areas locating along two neighboring lines of these hexagons [red and blue arrowed lines in Figs. 2(a) and 2(b)]. Among these hexagonal dark areas, half of them should exhibit the hexagonal current flux loops along one of the arrowed lines with a period of $2a_0$. The results measured on the neighboring line should not show any spin related signal. Figures 2(d) and 2(e) show tunneling spectra measured at centers of each hexagonal dark

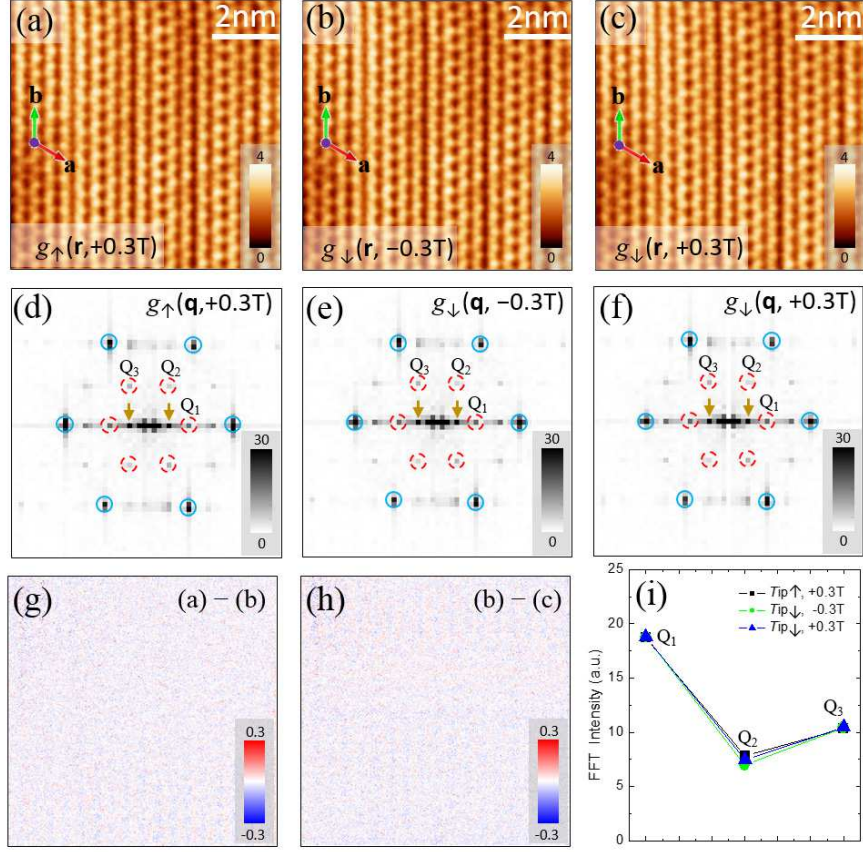


FIG. 3. (a)-(c) Differential conductance mappings measured at $E = 20$ meV in the same area ($V_{\text{set}} = 50$ mV, $I_{\text{set}} = 100$ pA). The magnetic field and the spin polarization of the tips are different in these configurations. (d) to (f) Fourier transform patterns of the differential conductance mappings in (a) to (c), respectively. (g),(h) Spin-difference differential conductance mappings derived by the subtraction of (b) from (a) and (c) from (b), respectively. (i) Intensities of scattering spots corresponding to the 2×2 CDW order in the FT pattern shown in (d) to (f).

areas along two neighboring routes as highlighted by the arrowed lines. The CDW gapped feature can be observed as two kinks at about ± 20 meV in the spectra, which is similar to a previous report [29]. Spin-difference spectra is calculated by the subtraction of two tunneling spectra measured at the same position but with different tip spin orientations and under different magnetic fields, and Fig. 2(f) shows the corresponding spin-difference spectra derived from those shown in Figs. 2(d) and 2(e). These spin-difference spectra are almost featureless and quite uniform at positions of hexagonal dark areas, disregard whether the measurement is taken on the line with or without the expected current flux loops. This indicates that our tunneling measurements with spin polarized tips do not show the signal arising from the expected chiral flux current phase.

C. Differential conductance mapping using spin-polarized tips

The differential conductance or the quasiparticle interference (QPI) mapping can provide more direct information of the spatial evolution of DOS. Figures 3(a)-3(c) show the differential conductance mappings measured with different tip spin orientations at different magnetic fields. There are also some stripes along b -axis direction in these QPI mappings, which is originated from the mixed contribution of the 1×4 unidirectional CDW order and the 2×2 CDW order. Figures 3(d)-3(f) show the corresponding FT patterns of Figs. 3(a)-3(c), respectively. The spots of the 2×2 CDW order can be seen clearly, and they are marked as Q_1 , Q_2 and Q_3 for different wave vectors. Obviously, the intensity of the Q_1 spots is stronger than the intensities of Q_2 and Q_3 spots. When we calculate the spin-difference signal between QPI mappings under different tip polarization directions and magnetic fields, the resultant spin-difference QPI mappings are shown in Figs. 3(g) and 3(h), indicating negligible

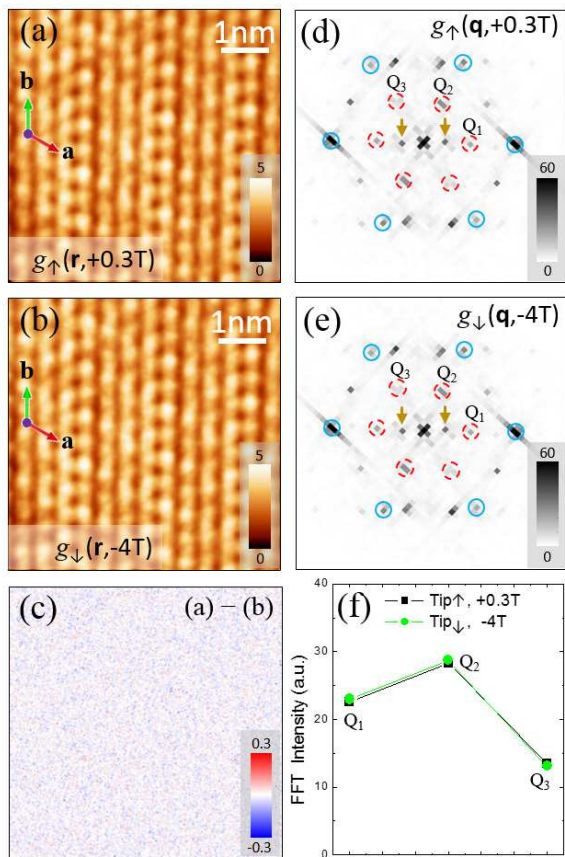


FIG. 4. (a),(b) Differential conductance mappings measured at $E = 20$ meV in the same area ($V_{\text{set}} = 30$ mV, $I_{\text{set}} = 100$ pA). The magnetic field and the spin polarization of the tips are different in these configurations. (c) Spin-difference differential conductance mappings derived by the subtraction of (b) from (a). (d),(e) Fourier transform patterns of the differential conductance mappings in (a) and (b), respectively. (f) Intensities of the FT patterns of the 2×2 CDW order shown in (d) and (e).

signal in this area. The difference QPI mappings exhibit featureless behavior not only for the proposed current flux loops but also for the 2×2 CDW order, and the latter rules out the possibility of attributing the gapped feature to the SDW order. To further investigate the possible spin texture of the 2×2 CDW order, we show the peak intensities of these spots in Fig. 3(i) from the FT patterns in Figs. 3(d)-3(f). Obviously, the differences of peak intensities are also very small for the spots measured with opposite tip polarization orientations and magnetic field directions. This shows again no indication of the spin texture of the chiral flux current phase with the resolution of our technique.

It should be noted that the chiral charge order was claimed by observing the variation of the intensities of some FT-spots corresponding to the 2×2 CDW order by applying a magnetic field of 2 T in KV_3Sb_5 [40] or 3 T in RbV_3Sb_5 [51]. One may argue that the unobserved spin

texture corresponding to the possible chiral charge order mentioned above in our experiments may be because the applied magnetic field of 0.3 T is too small, so a large magnetic field of 4 T is applied to investigate the spin-difference signal. Obviously, a higher magnetic field is supposed to be more effective to tune the direction of the magnetic moment arising from the current flux loops or the chiral charge order. Figure 4 shows the related results measured under magnetic fields of -4 and $+0.3$ T. The tip is polarized by the magnetic field of -4 and $+2$ T, respectively, in order to have the opposite directions of the tip spin. And the QPI data are recorded at -4 and $+0.3$ T in order to induce local moments with different orientations and magnitudes. The magnetic field of 4 T is supposed to be strong enough to induce a visible difference among the related FT-QPI spots which were attributed to the chiral charge order [40, 51]. From our data shown in Fig. 4(c), one can see that, however, there is no obvious feature in the spin-difference QPI mapping. In addition, the spot intensities of the FT-QPI patterns depicted in Fig. 4(f) show also negligible difference.

IV. DISCUSSION

By doing SP-STM/STS measurements in CsV_3Sb_5 , we have not observed any trace of the chiral flux current phase or the tunable chiral charge order in our experiment. One most possible reason would be that the resolution of our technique may not be high enough to resolve this phase. However, we must mention that, using the same technique we have successfully visualized an emergent incommensurate AF order in the nearby region of magnetic Fe impurities embedded in the optimally doped $\text{Bi}_2\text{Sr}_2\text{CaCu}_2\text{O}_{8+\delta}$ and the AF order in Fe_{1+y}Te [61], which proves the ability to detect the local magnetic moment by a spin-polarized Cr tip. The absence of spin-difference signal in CsV_3Sb_5 may be the intrinsic feature of this material. Here in this family of materials, the chiral flux current phase is proposed to explain the time-reversal symmetry breaking along c -axis direction [56] and the observation of the anomalous Hall effect [54, 55]. However, the μSR experiments show that the enhanced signal of the spin relaxation rate below the CDW temperature is mainly contributed by the nuclear magnetic moment at zero field or a small field lower than 1 T [57, 66], but rather than that from the chiral flux current phase. Hence, the absence of spin-difference signal from our experimental data measured at ± 0.3 T is understandable. In addition, we have not observed the tunable intensity of the 2×2 CDW spots at different magnetic fields up to 4 T with different directions of the tip spin, which is consistent with a recent report [49]. It seems that the 2×2 CDW order does not have the spin texture corresponding to the proposed chiral charge order from our SP-STM/STS measurements. From a recent μSR measurement [66], a factor of six enhancement of the spin relaxation rate at 8 T compared to zero-field

is observed in KV_3Sb_5 , this field is actually much higher than the saturation field (~ 1 T) of the AHE, which poses a question that whether the enhanced spin relaxation signal under a high field is really resulted from the chiral charge order. Our experiments give no indication of this chiral charge order. Certainly this remains still as an unsettled issue, more refined experiments are highly desired.

V. CONCLUSION

By using spin polarized tips, we have carried out careful measurements of scanning tunneling microscopy and spectroscopy on the recently discovered kagome metal CsV_3Sb_5 . Although our data reveal clear evidence of the 2×2 and 1×4 CDW orders, but refined analyses give no trace for the existence of the proposed chiral charge order or chiral current flux phase. This conclusion is drawn from the results of many thoughtful measurements and analyses: from both the absence of distinction between the spectra with and without the theoretically predicted local magnetic moments on neighboring hexagons of vanadium atoms, and negligible intensity difference

of the Fourier transform spots under different magnetic fields with different tip polarization directions.

ACKNOWLEDGMENTS

We appreciate the useful message concerning the technique of spin polarized tunneling measurement from Roland Wiesendanger. This work was supported by National Natural Science Foundation of China (Grants No. 11927809, No. 11974171, No. 12061131001, No. 92065109, No. 11734003, and No. 11904294), National Key R&D Program of China (Grant No. 2020YFA0308800), Strategic Priority Research Program (B) of Chinese Academy of Sciences (Grant No. XDB25000000), Beijing Natural Science Foundation (Grant No. Z190006), and Beijing Institute of Technology Research Fund Program for Young Scholars (Grant No. 3180012222011). Z.W. would like to thank Micro-nano Center at BIT for the assistance of sample characterization.

* These authors contributed equally to this work.

† huanyang@nju.edu.cn

‡ hhwen@nju.edu.cn

-
- [1] S. Sachdev, *Kagomé- and Triangular-Lattice Heisenberg Antiferromagnets: Ordering from Quantum Fluctuations and Quantum-Disordered Ground States with Unconfined Bosonic Spinons*, Phys. Rev. B. **45**, 12377 (1992).
- [2] L. Balents, *Spin Liquids in Frustrated Magnets*, Nature (London) **464**, 199 (2010).
- [3] S. Yan, D. A. Huse, and S. R. White, *Spin-Liquid Ground State of the $S = 1/2$ Kagome Heisenberg Antiferromagnet*, Science **332**, 1173 (2011).
- [4] T.-H. Han, J. S. Helton, S. Chu, D. G. Nocera, J. A. Rodriguez-Rivera, C. Broholm, and Y. S. Lee, *Fractionalized Excitations in the Spin-Liquid State of a Kagome-lattice Antiferromagnet*, Nature (London) **492**, 406 (2012).
- [5] S. Nakatsuji, N. Kiyohara, and T. Higo, *Large Anomalous Hall effect in a Non-Collinear Antiferromagnet at Room Temperature*, Nature (London) **527**, 212 (2015).
- [6] A. K. Nayak, J. E. Fischer, Y. Sun, B. Yan, J. Karel, A. C. Komarek, C. Shekhar, N. Kumar, W. Schnelle, J. Kübler, C. Felser, and S. S. P. Parkin, *Large Anomalous Hall Effect Driven by a Nonvanishing Berry Curvature in the Noncollinear Antiferromagnet Mn_3Ge* , Sci. Adv. **2**, e1501870 (2016).
- [7] E. Liu, Y. Sun, N. Kumar, L. Muechler, A. Sun, L. Jiao, S.-Y. Yang, D. Liu, A. Liang, Q. Xu, J. Kroder, V. Süß, H. Borrmann, C. Shekhar, Z. Wang, C. Xi, W. Wang, W. Schnelle, S. Wirth, Y. Chen, S. T. B. Goennenwein, and C. Felser, *Giant Anomalous Hall Effect in a Ferromagnetic Kagome-Lattice Semimetal*, Nat. Phys. **14**, 1125 (2018).
- [8] Q. Wang, Y. Xu, R. Lou, Z. Liu, M. Li, Y. Huang, D. Shen, H. Weng, S. Wang, and H. Lei, *Large Intrinsic Anomalous Hall Effect in Half-Metallic Ferromagnet $Co_3Sn_2S_2$ with Magnetic Weyl Fermions*, Nat. Commun. **9**, 3681 (2018).
- [9] H.-M. Guo and M. Franz, *Topological Insulator on the Kagome Lattice*, Phys. Rev. B **80**, 113102 (2009).
- [10] W.-S. Wang, Z.-Z. Li, Y.-Y. Xiang, and Q.-H. Wang, *Competing Electronic Orders on Kagome Lattices at Van Hove Filling*, Phys. Rev. B **87**, 115135 (2013).
- [11] W.-H. Ko, P. A. Lee, and X.-G. Wen, *Doped Kagome System as Exotic Superconductor*, Phys. Rev. B **79**, 214502 (2009).
- [12] M. L. Kiesel, C. Platt, and R. Thomale, *Unconventional Fermi Surface Instabilities in the Kagome Hubbard Mode*, Phys. Rev. Lett. **110**, 126405 (2013).
- [13] I. I. Mazin, H. O. Jeschke, F. Lechermann, H. Lee, M. Fink, R. Thomale, and R. Valenti, *Theoretical Prediction of a Strongly Correlated Dirac Metal*, Nat. Commun. **5**, 4261 (2014).
- [14] L. Ye, M. Kang, J. Liu, F. Cube, C. R. Wicker, T. Suzuki, C. Jozwiak, A. Bostwick, E. Rotenberg, D. C. Bell, L. Fu, R. Comin, and J. G. Checkelsky, *Massive Dirac Fermions in a Ferromagnetic Kagome Metal*, Nature (London) **555**, 638 (2018).
- [15] J.-X. Yin, S. S. Zhang, G. Chang, Q. Wang, S. S. Tsirkin, Z. Guguchia, B. Lian, H. Zhou, K. Jiang, I. Belopolski, N. Shumiya, D. Multer, M. Litskevich, T. A. Cochran, H. Lin, Z. Wang, T. Neupert, S. Jia, H. Lei, and M. Z. Hasan, *Negative Flat Band Magnetism in a Spin-Orbit-Coupled Correlated Kagome Magnet*, Nat. Phys. **15**, 443 (2019).
- [16] D. F. Liu, A. J. Liang, E. K. Liu, Q. N. Xu, Y. W. Li, C. Chen, D. Pei, W. J. Shi, S. K. Mo, P. Dudin, T. Kim, C. Chacho, G. Li, Y. Sun, L. X. Yang, Z. K. Liu, S. S. P. Parkin, C. Felser, and Y. L. Chen, *Magnetic Weyl*

- Semimetal Phase in a Kagomé Crystal*, Science **365**, 1282 (2019).
- [17] Z. Liu, M. Li, Q. Wang, G. Wang, C. Wen, K. Jiang, X. Lu, S. Yan, Y. Huang, D. Shen, J.-X. Yin, Z. Wang, Z. Yin, H. Lei, and S. Wang, *Orbital-Selective Dirac Fermions and Extremely Flat Bands in Frustrated Kagome-Lattice Metal CoSn*, Nat. Commun. **11**, 4002 (2020).
- [18] M. Kang, L. Ye, S. Fang, J.-S. You, A. Levitan, M. Han, J. I. Facio, C. Jozwiak, A. Bostwick, E. Rotenberg, M. K. Chan, R. D. McDonald, D. Graf, K. Kaznatcheev, Elio Vescovo, D. C. Bell, E. Kaxiras, J. Brink, M. Richter, M. P. Ghimire, J. G. Checkelsky, and R. Comin, *Dirac Fermions and Flat Bands in the Ideal Kagome Metal FeSn*, Nat. Mater. **19**, 163 (2020).
- [19] S.-L. Yu and J.-X. Li, *Chiral Superconducting Phase and Chiral Spin-Density-Wave Phase in a Hubbard Model on the Kagome Lattice*, Phys. Rev. B **85**, 144402 (2012).
- [20] B. R. Ortiz, L. C. Gomes, J. R. Morey, M. Winiarski, M. Bordelon, J. S. Mangum, I. W. H. Oswald, J. A. Rodriguez-Rivera, J. R. Neilson, S. D. Wilson, E. Ertekin, T. M. McQueen, and E. S. Toberer, *New Kagome Prototype Materials: Discovery of KV₃Sb₅, RbV₃Sb₅, and CsV₃Sb₅*, Phys. Rev. Mater. **3**, 094407 (2019).
- [21] B. R. Ortiz, S. M. L. Teicher, Y. Hu, J. L. Zuo, P. M. Sarte, E. C. Schueller, A. M. M. Abeykoon, M. J. Krogstad, S. Rosenkranz, R. Osborn, R. Seshadri, L. Balents, J. He, and S. D. Wilson, *CsV₃Sb₅: A Z₂ Topological Kagome Metal with a Superconducting Ground State*, Phys. Rev. Lett. **125**, 247002 (2020).
- [22] Q. Yin, Z. Tu, C. Gong, Y. Fu, S. Yan, and H. Lei, *Superconductivity and Normal-State Properties of Kagome Metal RbV₃Sb₅ Single Crystals*, Chin. Phys. Lett. **38**, 037403 (2021).
- [23] B. R. Ortiz, P. M. Sarte, E. M. Kenney, M. J. Graf, S. M. L. Teicher, R. Seshadri, and S. D. Wilson, *Superconductivity in the Z₂ Kagome Metal KV₃Sb₅*, Phys. Rev. Mater. **5**, 034801 (2021).
- [24] Y. Wang, S. Yang, P. K. Sivakumar, B. R. Ortiz, S. M. L. Teicher, H. Wu, A. K. Srivastava, C. Garg, D. Liu, S. S. P. Parkin, E. S. Toberer, T. McQueen, S. D. Wilson, and M. N. Ali, *Proximity-Induced Spin-Triplet Superconductivity and Edge Supercurrent in the Topological Kagome Metal, K_{1-x}V₃Sb₅*, arXiv:2012.05898.
- [25] C. C. Zhao, L. S. Wang, W. Xia, Q. W. Yin, J. M. Ni, Y. Y. Huang, C. P. Tu, Z. C. Tao, Z. J. Tu, C. S. Gong, H. C. Lei, Y. F. Guo, X. F. Yang, and S. Y. Li, *Nodal Superconductivity and Superconducting Domes in the Topological Kagome Metal CsV₃Sb₅*, arXiv:2102.08356.
- [26] K. Y. Chen, N. N. Wang, Q. W. Yin, Y. H. Gu, K. Jiang, Z. J. Tu, C. S. Gong, Y. Uwatoko, J. P. Sun, H. C. Lei, J. P. Hu, and J.-G. Cheng, *Double Superconducting Dome and Triple Enhancement of T_c in the Kagome Superconductor CsV₃Sb₅ under High Pressure*, Phys. Rev. Lett. **126**, 247001 (2021).
- [27] Z. Zhang, Z. Chen, Y. Zhou, Y. Yuan, S. Wang, J. Wang, H. Yang, C. An, L. Zhang, X. Zhu, Y. Zhou, X. Chen, J. Zhou, and Z. Yang, *Pressure-Induced Reemergence of Superconductivity in the Topological Kagome Metal CsV₃Sb₅*, Phys. Rev. B **103**, 224513 (2021).
- [28] X. Chen, X. Zhan, X. Wang, J. Deng, X.-B. Liu, X. Chen, J.-G. Guo, and X. Chen, *Highly Robust Reentrant Superconductivity in CsV₃Sb₅ under Pressure*, Chin. Phys. Lett. **38**, 057402 (2021).
- [29] Z. Liang, X. Hou, W. Ma, F. Zhang, P. Wu, Z. Zhang, F. Yu, J.-J. Ying, K. Jiang, L. Shan, Z. Wang, and X.-H. Chen, *Three-Dimensional Charge Density Wave and Robust Zero-Bias Conductance Peak inside the Superconducting Vortex Core of a Kagome Superconductor CsV₃Sb₅*, arXiv:2103.04760.
- [30] H. Chen, H. Yang, B. Hu, Z. Zhao, J. Yuan, Y. Xing, G. Qian, Z. Huang, G. Li, Y. Ye, Q. Yin, C. Gong, Z. Tu, H. Lei, S. Ma, H. Zhang, S. Ni, H. Tan, C. Shen, X. Dong, B. Yan, Z. Wang, and H.-J. Gao, *Roton Pair Density Wave and Unconventional Strong-Coupling Superconductivity in a Topological Kagome Metal*, arXiv:2103.09188.
- [31] W. Duan, Z. Nie, S. Luo, F. Yu, B. R. Ortiz, L. Yin, H. Su, F. Du, A. Wang, Y. Chen, X. Lu, J. Ying, S. D. Wilson, X. Chen, Y. Song, and H. Yuan, *Nodeless Superconductivity in the Kagome Metal CsV₃Sb₅*, arXiv:2103.11796.
- [32] J. Zhao, W. Wu, Y. Wang, and S. A. Yang, *Electronic Correlations in the Normal State of the Kagome Superconductor KV₃Sb₅*, Phys. Rev. B **103**, L241117 (2021).
- [33] S. Ni, S. Ma, Y. Zhang, J. Yuan, H. Yang, Z. Lu, N. Wang, J. Sun, Z. Zhao, D. Li, S. Liu, H. Zhang, H. Chen, K. Jin, J. Cheng, L. Yu, F. Zhou, X. Dong, J. Hu, H.-J. Gao, and Z. Zhao, *Anisotropic Superconducting Properties of Kagome Metal CsV₃Sb₅*, Chin. Phys. Lett. **38**, 057403 (2021).
- [34] X. Wu, T. Schwemmer, T. Müller, A. Consiglio, G. Sangiovanni, D. D. Sante, Y. Iqbal, W. Hanke, A. P. Schnyder, M. M. Denner, M. H. Fischer, T. Neupert, and R. Thomale, *Nature of Unconventional Pairing in the Kagome Superconductors AV₃Sb₅*, arXiv:2104.05671.
- [35] C. Mu, Q. Yin, Z. Tu, C. Gong, H. Lei, Z. Li, and J. Luo, *s-Wave Superconductivity in Kagome Metal CsV₃Sb₅ Revealed by ^{121/123}Sb NQR and ⁵¹V NMR Measurements*, arXiv:2104.06698.
- [36] H.-S. Xu, Y.-J. Yan, R. Yin, W. Xia, S. Fang, Z. Chen, Y. Li, W. Yang, Y. Guo, and D.-L. Feng, *Multiband Superconductivity with Sign-Preserving Order Parameter in Kagome Superconductor CsV₃Sb₅*, arXiv:2104.08810.
- [37] Y. Fu, N. Zhao, Z. Chen, Q. Yin, Z. Tu, C. Gong, C. Xi, X. Zhu, Y. Sun, K. Liu, and H. Lei, *Quantum Transport Evidence of Topological Band Structures of Kagome Superconductor CsV₃Sb₅*, arXiv:2104.08193.
- [38] K. Nakayama, Y. Li, M. Liu, Z. Wang, T. Takahashi, Y. Yao, and T. Sato, *Multiple Energy Scales and Anisotropic Energy Gap in the Charge-Density-Wave Phase of Kagome Superconductor CsV₃Sb₅*, arXiv:2104.08042.
- [39] M. Kang, S. Fang, J.-K. Kim, B. R. Ortiz, J. Yoo, B.-G. Park, S. D. Wilson, J.-H. Park, and R. Comin, *Twofold Van Hove Singularity and Origin of Charge Order in Topological Kagome Superconductor CsV₃Sb₅*, arXiv:2105.01689.
- [40] Y.-X. Jiang, J.-X. Yin, M. M. Denner, N. Shumiya, B. R. Ortiz, G. Xu, Z. Guguchia, J. He, M. S. Hossain, X. Liu, J. Ruff, L. Kautzsch, S. S. Zhang, G. Chang, I. Belopolski, Q. Zhang, T. A. Cochran, D. Multer, M. Litskevich, Z.-J. Cheng, X. P. Yang, Z. Wang, R. Thomale, T. Neupert, S. D. Wilson, and M. Z. Hasan, *Unconventional Chiral Charge Order in Kagome Superconductor KV₃Sb₅*, Nat. Mater. DOI:10.1038/s41563-021-01034-y (2021).
- [41] H. Zhao, H. Li, B. R. Ortiz, S. M. L. Teicher, T. Park, M. Ye, Z. Wang, L. Balents, S. D. Wilson, and I. Zeljkovic, *Cascade of Correlated Electron States in a Kagome Su-*

- perconductor CsV₃Sb₅, arXiv:2103.03118.
- [42] H. Tan, Y. Liu, Z. Wang, and B. Yan, *Charge Density Waves and Electronic Properties of Superconducting Kagome Metals*, arXiv:2103.06325.
- [43] E. Uykur, B. R. Ortiz, S. D. Wilson, M. Dressel, and A. A. Tsirlin, *Optical Detection of Charge-Density-Wave Instability in the Non-Magnetic Kagome Metal KV₃Sb₅*, arXiv:2103.07912.
- [44] H. X. Li, T. T. Zhang, Y.-Y. Pai, C. Marvinney, A. Said, T. Yilmaz, Q. Yin, C. Gong, Z. Tu, E. Vescovo, R. G. Moore, S. Murakami, H. C. Lei, H. N. Lee, B. Lawrie, and H. Miao, *Observation of Unconventional Charge Density Wave without Acoustic Phonon Anomaly in Kagome Superconductors AV₃Sb₅ (A = Rb, Cs)*, arXiv:2103.09769.
- [45] M. M. Denner, R. Thomale, and T. Neupert, *Analysis of Charge Order in the Kagome Metal AV₃Sb₅ (A=K, Rb, Cs)*, arXiv:2103.14045.
- [46] X. Zhou, Y. Li, X. Fan, J. Hao, Y. Dai, Z. Wang, Y. Yao, and H.-H. Wen, *Origin of Charge Density Wave in the Kagome Metal CsV₃Sb₅ as Revealed by Optical Spectroscopy*, Phys. Rev. B **104**, L041101 (2021).
- [47] Y.-P. Lin and R. M. Nandkishore, *Complex Charge Density Waves at Van Hove Singularity on Hexagonal Lattices: Haldane-Model Phase Diagram and Potential Realization in Kagome Metals AV₃Sb₅*, arXiv:2104.02725
- [48] Z. Wang, S. Ma, Y. Zhang, H. Yang, Z. Zhao, Y. Ou, Y. Zhu, S. Ni, Z. Lu, H. Chen, K. Jiang, L. Yu, Y. Zhang, X. Dong, J. Hu, H.-J. Gao, and Z. Zhao, *Distinctive Momentum Dependent Charge-Density-Wave Gap Observed in CsV₃Sb₅ Superconductor with Topological Kagome Lattice*, arXiv:2104.05556.
- [49] H. Li, H. Zhao, B. R. Ortiz, T. Park, M. Ye, L. Balents, Z. Wang, S. D. Wilson, and I. Zeljkovic, *Rotation Symmetry Breaking in the Normal state of a Kagome Superconductor KV₃Sb₅*, arXiv:2104.08209.
- [50] T. Park, M. Ye, and L. Balents, *Electronic Instabilities of Kagome Metals: Saddle Points and Landau Theory*, arXiv:2104.08425.
- [51] N. Shumiya, M. S. Hossain, J.-X. Yin, Y.-X. Jiang, B. R. Ortiz, H. Liu, Y. Shi, Q. Yin, H. Lei, S. S. Zhang, G. Chang, Q. Zhang, T. A. Cochran, D. Multer, M. Litskevich, Z.-J. Cheng, X. P. Yang, Z. Guguchia, S. D. Wilson, and M. Z. Hasan, *Tunable Chiral Charge Order in Kagome Superconductor RbV₃Sb₅*, arXiv:2105.00550.
- [52] Z. Wang, Y.-X. Jiang, J.-X. Yin, Y. Li, G.-Y. Wang, H.-L. Huang, S. Shao, J. Liu, P. Zhu, N. Shumiya, M. S. Hossain, H. Liu, Y. Shi, J. Duan, X. Li, G. Chang, P. Dai, Z. Ye, G. Xu, Y. Wang, H. Zheng, J. Jia, M. Z. Hasan, and Y. Yao, *Electronic Nature of Chiral Charge Order in Kagome Superconductor CsV₃Sb₅*, arXiv:2105.04542.
- [53] Y. Luo, S. Peng, S. M. L. Teicher, L. Huai, Y. Hu, B. R. Ortiz, Z. Wei, J. Shen, Z. Ou, B. Wang, Y. Miao, M. Guo, M. Shi, S. D. Wilson, and J.-F. He, *Distinct Band Reconstructions in Kagome Superconductor CsV₃Sb₅*, arXiv:2106.01248.
- [54] S.-Y. Yang, Y. Wang, B. R. Ortiz, D. Liu, J. Gayles, E. Derunova, R. Gonzalez-Hernandez, L. Šmejkal, Y. Chen, S. S. P. Parkin, S. D. Wilson, E. S. Toberer, T. McQueen, and M. N. Ali, *Giant, Unconventional Anomalous Hall effect in the Metallic Frustrated Magnet Candidate, KV₃Sb₅*, Sci. Adv. **6**, eabb6003 (2020).
- [55] F. H. Yu, T. Wu, Z. Y. Wang, B. Lei, W. Z. Zhuo, J. J. Ying, and X. H. Chen, *Concurrence of Anomalous Hall Effect and Charge Density Wave in a Superconducting Topological Kagome Metal*, Phys. Rev. B **104**, L041103 (2021).
- [56] X. Feng, K. Jiang, Z. Wang, and J. Hu, *Chiral Flux Phase in the Kagome Superconductor AV₃Sb₅*, Sci. Bull. DOI:10.1016/j.scib.2021.04.043 (2021).
- [57] E. M. Kenney, B. R. Ortiz, C. Wang, S. D. Wilson, and M. J. Graf, *Absence of Local Moments in the Kagome Metal KV₃Sb₅ as Determined by Muon Spin Spectroscopy*, J. Phys: Condens. Matter **33**, 235801 (2021).
- [58] Y. Xiang, Q. Li, Y. Li, W. Xie, H. Yang, Z. Wang, Y. Yao, and H.-H. Wen, *Twofold Symmetry of c-Axis Resistivity in Topological Kagome Superconductor CsV₃Sb₅ with in-Plane Rotating Magnetic Field*, arXiv:2104.06909.
- [59] A. Schlenhoff, S. Krause, G. Herzog, and R. Wiesendanger, *Bulk Cr Tips with Full Spatial Magnetic Sensitivity for Spin-Polarized Scanning Tunneling Microscopy*, Appl. Phys. Lett. **97**, 083104 (2010).
- [60] D. Huang, S. Liu, I. Zeljkovic, J. F. Mitchell, and J. E. Hoffman, *Etching of Cr Tips for Scanning Tunneling Microscopy of Cleavable Oxides*, Rev. Sci. Instrum. **88**, 023705 (2017).
- [61] S. Wan, H. Li, P. Choubey, Q. Gu, H. Li, H. Yang, I. Eremin, G. D. Gu, and H.-H. Wen, *Direct Visualization of a Static Incommensurate Antiferromagnetic Order by Suppressing the Superconducting Phase Coherence in Fe-Doped Bi₂Sr₂CaCu₂O_{8+δ}*, arXiv:2107.09967.
- [62] J. E. Hoffman, *Spectroscopic Scanning Tunneling Microscopy Insights into Fe-Based Superconductors*, Rep. Prog. Phys. **47**, 124513 (2011).
- [63] R. Wiesendanger, *Spin Mapping at the Nanoscale and Atomic Scale*, Rev. Mod. Phys. **81**, 1495 (2009).
- [64] M. Enayat, Z. Sun, U. R. Singh, R. Aluru, S. Schmaus, A. Yaresko, Y. Liu, C. Lin, V. Tsurkan, A. Loidl, J. Deisenhofer, and P. Wahl, *Real-Space Imaging of the Atomic-Scale Magnetic Structure of Fe_{1+y}Te*, Science **345**, 653 (2014).
- [65] N. Nagaosa, J. Sinova, S. Onoda, A. H. MacDonald, and N. P. Ong, *Anomalous Hall Effect*, Rev. Mod. Phys. **82**, 1539 (2010).
- [66] C. Mielke III, D. Das, J.-X. Yin, H. Liu, R. Gupta, C. N. Wang, Y.-X. Jiang, M. Medarde, X. Wu, H. C. Lei, J. J. Chang, P. Dai, Q. Si, H. Miao, R. Thomale, T. Neupert, Y. Shi, R. Khasanov, M. Z. Hasan, H. Luetkens, and Z. Guguchia, *Time-Reversal Symmetry-Breaking Charge Order in a Correlated Kagome Superconductor*, arXiv:2106.13443.